PHYSICAL REVIEW B VOLUME 10, NUMBER 7 1 OCTOBER 1974

Feynman-graph theory of the Kondo effect. I. Exact summation of parquet graphs without divergences*†

W. S. Verwoerd
Department of Physics, University of Pretoria, Pretoria, Republic of South Africa
(Received 11 September 1973)

The Feynman-graph formalism is used to calculate the self-energy of conduction electrons exchange interacting with a single $S=1/2$ impurity atom, and hence the Kondo contribution to the resistivity R in dilute magnetic alloys. To eliminate the effect of spurious states that result from second quantization, we derive a new limiting procedure which satisfies the linked-cluster expansion and maintains a fixed impurity-spin magnitude. A novel set of diagrammatic equations is found which exactly sums the set of non-self-consistent parquet graphs without any multiple counting. The resulting integral equations are solved in an approximation which omits certain diagrams, but still sums the remainder exactly. The self-energy so obtained yields the simple form $R=2\pi^2 R_u[4\ln^2(T/T_K)+\pi^2]^{-1}$ for the resistivity R as a function of the temperature T, with R_u the unitarity limit and T_K the Kondo temperature. Although containing the results of various previous authors as approximations to it, this expression is free of the divergences found by them. While we succeed in eliminating the divergences by accurate summation, we find that the observed saturation of R at zero temperature is not given by a non-self-consistent calculation. The self-consistent case is covered in the following paper.

I. INTRODUCTION

A variety of distinct theoretical approaches have been applied to the Kondo effect: perturbation theory first applied by Abrikosov,[1] decoupled equations of motion by Nagaoka,[2] Chew-Low theory by Suhl,[3] and more recently the scaling approach reviewed by Anderson in Ref. 4.

Hamann[5] found an exact solution of Nagaoka's decoupled equations and obtained good agreement with experimental data for the resistivity of dilute magnetic alloys in the high-temperature limit. At low temperatures, the right qualitative behavior is obtained, but the resistivity does not saturate fast enough to the unitarity limit as the temperature decreases. Moreover, as pointed out by Zittartz and Müller-Hartmann,[6,7] the Nagaoka-Hamann equations do not satisfy the Mattiss singlet-ground-state theorem.[8]

In order to improve upon the Hamann solution, it is desirable to replace the rather intuitive decoupling approach by a more explicit approximation. One candidate is diagrammatic perturbation theory. The first application of this by Abrikosov[1] yields agreement with Hamann's work in the high-temperature region, but diverges at a Kondo temperature T_K. Below T_K, the resistivity approaches zero instead of saturating. Apart from this disagreement with both Hamann's results and experimental work, the Abrikosov treatment has been criticized by Keiter.[9] He points out that the projection procedure introduced by Abrikosov to get rid of spurious states (introduced by second quantization of the spin operator in the Kondo Hamiltonian), violates the linked-cluster theorem. There has been considerable discussion of this point in the recent literature[10–15] and we will return to it in Sec. II A.

These problems do not occur in the alternative diagrammatic treatment of Cheung and Mattuck[16] (CM). Instead of the Abrikosov projection procedure, CM uses a limiting procedure due to Takano and Ogawa[17] (TO), to which the linked-cluster theorem can be applied. First performing a sum of ladder-type parquet diagrams only, CM finds a diverging behavior similar to that of TO, and, like Abrikosov, a resistivity that vanishes at zero temperature. The inclusion of self-consistently-clothed propagators in the ladder summation removes the divergence and gives saturation at low temperatures according to essentially the same formula as that of Hamann.

In a systematic approximation the non-ladder parquet diagrams must also be included as their contributions are of the same order in the diverging logarithm as that of the ladder diagrams. Up to now no exact summation of the full parquet series has been performed. The approximate procedure of Abrikosov[1] is claimed, however, to be accurate to leading order in the logarithm, and is used subsequently by Silverstein and Duke.[18]

Cheung and Mattuck therefore conclude their work with an argument based on the results of Silverstein and Duke, to show that the bare and clothed versions of the full parquet approximation yield essentially the same results as the corresponding ladder diagram calculations—specifically the Hamann formula for a self-consistent computation. We see that the diagrammatic approach has converged to the same result as the decoupling approach, which is gratifying. However, the above-mentioned shortcomings of the Nagaoka-Hamann

theory persist.

It should also be pointed out that the physical model of the CM treatment is not exactly the same as that of Nagaoka. Nagaoka bases his calculation on the "pure" Kondo model in which the impurity-spin value S is fixed. The TO limiting procedure used by CM, on the other hand, allows both $S=\frac{1}{2}$ and $S=0$ values, although the correct average occupation number of spin-up and spin-down levels is maintained. That the two schemes are not equivalent, is illustrated by the fact that an extra divergence is found (in the bare propagator expansion) in both Refs. 16 and 17, which is absent in pure Kondo model calculations.

The present work is a diagrammatic theory based on a new limiting technique first outlined in Ref. 15. The linked-cluster theorem remains valid and a fixed spin value is maintained. Apart from the fact that this simplifies the algebra considerably, it means that our method can serve as a direct basis of comparison with decoupling and other pure Kondo model calculations. Our limiting procedure is discussed more fully in Sec. IIB.

The previous work outlined above makes it clear that the essential physical features of the Kondo system (at least at low temperatures) is not described accurately by only the leading order in the logarithm. It is therefore necessary to obtain a more refined summation of the parquet graphs than the Abrikosov procedure. The present work also attempts to do this. In fact, in Sec. IIIB we derive a set of diagrammatic equations which exactly sums the parquet series. However, for the sake of a simple solution of the resulting integral equation, we introduce an approximation which eliminates again certain parquet diagrams from the series. Still, the remainder of the series is nevertheless summed exactly.

The technicalities of our method are such that we find it advantageous to devote Sec. III to a calculation in zero-temperature formalism before we proceed in Sec. IV to our main purpose, the computation of the conduction-electron self-energy as a function of temperature. Despite some complicated algebra in intermediate stages, a very simple expression for this is found in Eq. (3.22) (as interpreted in Sec. IV).

Finally, in Sec. V, we calculate in various approximations the contribution of Kondo scattering to the resistivity. We start with third-order perturbation theory and progressively include larger classes of graphs until we arrive at the full parquet approximation for the self-energy. It is found that the non-self-consistent formulas of Kondo,[19] Cheung and Mattuck,[16] Nagaoka,[2] and Abrikosov[1] are all approximations to our expression for the resistivity, Eq. (5.13). By including also the terms of low order in the logarithmic divergence, our calculation is, moreover, free of divergence at the Kondo temperature, as shown by Fig. 10.

As is well known, it is observed that the resistivity of dilute magnetic alloys saturates at zero temperature. For any realistic order of magnitude of the interaction, our result approaches zero instead. In the following paper, we show that this difficulty is removed by making the present calculation self-consistent.

II. DESCRIPTION OF THE MODEL

A. Hamiltonian

The problem we study is the scattering of conduction electrons from a single-impurity atom with spin $\vec{S}$, located at the origin. The interaction Hamiltonian used by Kondo[19] for this system is

$$H_k' = -\frac{J}{N}\sum_{k'k}\left[(c_{k'\uparrow}^\dagger c_{k\uparrow} - c_{k'\downarrow}^\dagger c_{k\downarrow})S_z + c_{k'\uparrow}^\dagger c_{k\downarrow} S_- + c_{k'\downarrow}^\dagger c_{k\uparrow} S_+\right]. \tag{2.1}$$

Here $c_{k\uparrow}^\dagger$ creates an electron with spin-up in a conduction-electron state with momentum $\vec{k}$, etc.

We will classify all calculations (like Refs. 2 and 4) based on the interaction of Eq. (2.1) (which has a fixed magnitude S for the impurity spin) as pure Kondo model calculations.

Most diagrammatic calculations—e.g., Refs. 1, 16, 20, and the present work—are based on a second quantized version of Eq. (2.1). For $S=\frac{1}{2}$, this is given by[21]

$$H' = -\frac{J}{2N}\sum_{k,k',\sigma}(c_{k'\sigma}^\dagger c_{d\sigma}^\dagger c_{d\sigma} c_{k\sigma} - c_{k'\sigma}^\dagger c_{d-\sigma}^\dagger c_{d-\sigma} c_{k\sigma} + 2c_{k'\sigma}^\dagger c_{d-\sigma} c_{d\sigma} c_{k-\sigma}). \tag{2.2}$$

Here the label d represents an electron state (nondegenerate for $S=\frac{1}{2}$) that is localized on the impurity atom. We use this notation consistently, while the labels k, k', p, and q are used for conduction-electron (k-electron) states. The factor $1/2N$ (N representing the total number of atoms in the crystal) will be absorbed into the J for the sake of brevity.

The idealization in Eqs. (2.1) and (2.2) of an interaction strength J which is constant in momentum space (corresponding to a contact interaction) leads to a divergence when the sum over all momenta is performed. Like previous authors, we will avoid this by assuming a density of conduction states with the constant value ρ in a narrow band of width $2D$ centered about the Fermi energy ϵ_F, and zero elsewhere.

We can now show that H_K' and H' are not completely equivalent in perturbation theory. When H' is used as the perturbation, the applicable unperturbed Hamiltonian is

$$H_0 = \sum_{k,0} (\epsilon_k - \mu) c^\dagger_{k\sigma} c_{k\sigma} + \sum_\sigma (\epsilon_d - \mu_{d\sigma}) c^\dagger_{d\sigma} c_{d\sigma} . \tag{2.3}$$

Here ϵ_k and ϵ_d are single-particle energies, while the μ's are Lagrange multipliers, which can be adjusted to give the correct number of particles.

The second sum in Eq. (2.3) is the total unperturbed energy of the localized spin. In the pure Kondo model, it is a constant that can be omitted. However, in the diagrammatic perturbation-theory formalism, this term must be included in H_0, and its contribution varies according to the occupation number of the d states. At finite temperatures, ensemble averages are taken over the complete set of eigenstates of H_0. The impurity-spin component of this set consists of the states $|n_{d\uparrow}, n_{d\downarrow}\rangle = |1,0\rangle$, $|0,1\rangle$, $|0,0\rangle$, and $|1,1\rangle$. The first two of these have $S = \frac{1}{2}$ and correspond to the eigenstates in the pure Kondo model; the last two, having $S = 0$, are spurious and various proposals have been made for eliminating their influence by a choice of the extra parameters $(\epsilon_d - \mu_{d\sigma})$ which do not occur in the pure Kondo model.

The TO procedure,[16,17] mentioned in Sec. I, is based on the fact that the states with $S = 0$ gives zero contribution in the calculation of Green's functions, etc. The $\mu_{d\sigma}$ are chosen in such a way that $\epsilon_d - \mu_{d\sigma} = 0$, ensuring that the d state has an average occupation number $\langle n_d \rangle = \frac{1}{2}$. It is then only necessary to insert a numerical correction factor to compensate for the fact that the ensemble average is taken over four states instead of two.

A more general procedure that can be applied to any spin value was formulated by Abrikosov.[1] It makes use of the fact that we wish to keep the contributions of states with exactly one d electron (or pseudofermion for $S > \frac{1}{2}$). These give rise to diagrams with one d-electron hole line in the diagrammatic expansion of, for example, the Green's function. All diagrams with more than one hole line are then eliminated by multiplying the expansion by the factor $\exp\beta(\epsilon_d - \mu_d)$ and taking the limit $(\epsilon_d - \mu_d) \to +\infty$. However, as pointed out by Keiter,[9] this means that unlinked diagrams are eliminated from both the numerator and denominator of the Green's function, so that the cancellation on which the linked-cluster expansion is based, fails to occur.

B. New limiting procedure

For the reasons stated in Sec. I, our calculation will be based on yet another limiting procedure. While we discuss only the $S = \frac{1}{2}$ case, generalization to higher spin seems straightforward. We repeat here, in somewhat more detail, the arguments given in Ref. 14.

Consider first the zero-temperature propagator[22] $G_{\sigma\sigma'}(\vec{k}t, \vec{k}'t')$ in the pure Kondo model. This can be expressed [Eq. (8.9) of Ref. 22] as the quotient of two expectation values in the noninteracting ground state $|\Phi_0\rangle$, given by

$$|\Phi_0\rangle = |F_0\rangle |S\rangle . \tag{2.4}$$

Here $|F_0\rangle$ represents the ground state of the Fermi sea and $|S\rangle$ the impurity-spin state. We specify the direction of our z axis to be parallel to σ, the spin vector of the incoming particle in the propagator, and we abbreviate the state with $S_z = +\frac{1}{2}$ as $|\uparrow\rangle$. Without interaction, the states $|\uparrow\rangle$ and $|\downarrow\rangle$ are degenerate and $|S\rangle$ is a linear combination of these. The interaction H'_K lifts the degeneracy and in order to ensure a smooth transition when H'_K is switched on, we use the following form for H_0:

$$H_0 = \sum_{k\sigma} (\epsilon_k - \mu) c^\dagger_{k\sigma} c_{k\sigma} + \lim_{\lambda \to 0} \lambda H'_k . \tag{2.5}$$

The full set of eigenstates of Eq. (2.5) is the set

$$E = \{ |F_i\rangle |\uparrow\rangle, \ |F_i\rangle |\downarrow\rangle \} , \tag{2.6}$$

where i ranges over the ground state and all excited states of the Fermi sea. With H_0 taken as in Eq. (2.5) the spin component of $|\Phi_0\rangle$ is now uniquely determined as either $|\uparrow\rangle$ or $|\downarrow\rangle$, depending on the sign of the coupling constant J. A distinct zero-temperature propagator will be obtained for each case, which we denote by $G_\uparrow$ and $G_\downarrow$ for $J > 0$ and $J < 0$, respectively.

Next we turn to the finite-temperature single-particle propagator $\mathcal{G}$, still working in the pure Kondo model. $\mathcal{G}$ is the quotient of two traces [Eq. (24.13) of Ref. 22], each performed over the set E. It is seen from Eq. (2.6) that the sum implied by the trace operation, can be split into two contributions. Each contribution involves a specific impurity-spin state, but is a weighted average over all the Fermi sea states. The denominator of $\mathcal{G}$, for example, is then given by $(V_\uparrow + V_\downarrow)$ where $V_\uparrow$ is the finite-temperature vacuum amplitude evaluated as a thermodynamic average over the ensemble of Fermi sea states, but assuming a fixed $|S\rangle = |\uparrow\rangle$ state. A similar expression applies to the numerator. Note that the temperature dependence is contained in the thermodynamic weighting factor, which is expressed in terms of the noninteracting Hamiltonian H_0. From Eq. (2.5) it is clear that the impurity spin gives a negligible contribution, so that the full temperature dependence is furnished by the Fermi sea.

A diagrammatic series expansion of each of the two vacuum amplitudes can now be given by the standard procedure,[23] provided that we discard the pure Kondo model by substituting H' for H'_K. Similarly to the vacuum amplitude, each of the two terms in the numerator of $\mathcal{G}$ can be expressed as a

sum of diagrams to which the linked-cluster theorem is applicable, so that we obtain

$$\mathcal{G} = (C_\uparrow V_\downarrow + C_\downarrow V_\downarrow)/(V_\uparrow + V_\downarrow), \tag{2.7}$$

where C represents the sum of all linked-cluster diagrams.

As long as the Fermi sea is isotropic, there is no direction of preference for the impurity spin and $V_\uparrow = V_\downarrow$. This can also be proved more explicity in terms of the diagrammatic expansion by making use of the equality of conjugate diagrams (see Sec. III C) which we will derive in Appendix A.

Equation (2.7) can consequently be reduced to

$$\mathcal{G} = \tfrac{1}{2}(\mathcal{G}_\uparrow + \mathcal{G}_\downarrow), \tag{2.8}$$

where $\mathcal{G}_\uparrow$ is the linked-cluster single-particle propagator in a system with an impurity-spin fixed in the positive z direction. The importance of Eq. (2.8) is that we can formulate a simple limiting procedure for the exact diagrammatic calculation of $\mathcal{G}_\uparrow$ and $\mathcal{G}_\downarrow$. The standard formalism yields the single-particle propagator obtained from an ensemble containing unperturbed systems with all four possible occupations of the d states. For the calculation of $\mathcal{G}_\uparrow$, for example, the ensemble must be restricted to systems with $|n_{d\uparrow}, n_{d\downarrow}\rangle = |1, 0\rangle$. Recalling the unperturbed expectation value

$$\langle n_{d\uparrow}\rangle = [\exp\beta(\epsilon_d - \mu_{d\uparrow}) + 1]^{-1}, \tag{2.9}$$

it is clear that this can be done by the choice

$$\epsilon_d - \mu_{d\uparrow} = -U, \quad \epsilon_d - U_{d\downarrow} = +U \tag{2.10}$$

and by taking the limit $U \to +\infty$. Similarly $\mathcal{G}_\downarrow$ is calculated by finding the single-particle propagator from some linked-cluster expansion and then taking the limit $U \to -\infty$.

It will be seen in Sec. IV A that we have to modify this limiting procedure slightly when applied to calculations in momentum space.

C. Calculation of the resistivity

In the relaxation-time approximation[24] the resistivity R of a metal is given by

$$R = 3(e^2\rho v^2\tau)^{-1}\big|_{\epsilon=\epsilon_F}, \tag{2.11}$$

where ρ is the density of states, v the velocity, and τ the relaxation time for conduction electrons with energy ϵ.

The relaxation time τ can be expressed in terms of the single-particle transition matrix T of scattering theory. Making use of the fact that our scattering potential H' is a contact interaction, and of the optical theorem, we obtain

$$1/\tau = -2\,\mathrm{Im}\,T_{qq}, \tag{2.12}$$

with q on the Fermi surface.

Assuming that the concentration c of impurity atoms is low enough that the contribution of each to the resistivity is additive, we thus find

$$R = \tfrac{1}{2}\pi\rho R_u(-2\,\mathrm{Im}\,T_{qq})\big|_{\epsilon_q=\epsilon_F}, \tag{2.13}$$

$$R_u = 6cN/\pi e^2\rho^2 v_F^2. \tag{2.14}$$

Here R_u is the unitarity limit resistivity and N the total number of atoms in the crystal.

The connection with the propagator formalism is made by noticing that the single-particle T matrix is simply the reducible self-energy evaluated on the energy shell. This is expressed by

$$T_{kk'}(\omega) = \frac{\Sigma_{kk'}(\omega)}{1 - \sum_p \mathcal{G}_0(p, \omega)\,\Sigma_{kp}(\omega)}, \tag{2.15}$$

where Σ represents the self-energy, while the Dyson equation for the propagator in momentum space takes the form

$$\mathcal{G}(k, k', \omega) = \mathcal{G}_0(k, \omega)\delta_{kk'} + \mathcal{G}_0(k, \omega)T_{kk'}(\omega)\mathcal{G}_0(k', \omega). \tag{2.16}$$

The symbol $\mathcal{G}_0$ represents the unperturbed propagator.

Application of Eq. (2.16) to each of the three propagators in Eq. (2.8) yields the result

$$T(\omega) = \tfrac{1}{2}[T_\uparrow(\omega) + T_\downarrow(\omega)]. \tag{2.17}$$

As before, the arrow subscripts indicate fixed impurity-spin ground states. Because the interaction strength J is independent of momentum, both the self-energy and the T matrix are independent of their momentum subscripts which are omitted in Eq. (2.17) and henceforth. Combining Eqs. (2.13) and (2.17) it is found that

$$R/R_u = -\tfrac{1}{2}\pi\rho\,\mathrm{Im}[T_\uparrow(\omega) + T_\downarrow(\omega)]\big|_{\omega=\epsilon_F}. \tag{2.18}$$

III. SELF-ENERGY AT ZERO TEMPERATURE

Before proceeding to the finite-temperature conduction or k-electron self-energy, it is useful to calculate Σ in the zero-temperature formalism. There is, of course, a close analogy between the two calculations, and making use of this we will be able to simplify considerably the finite temperature calculation in Sec. IV.

A. Conventions in diagrams

Like previous authors, we use solid lines for k-electron propagators and a broken line for the d-electron propagator. One of the simplest contributions to the k-electron propagator is then represented by Fig. 1(a).

The diagram of Fig. 1(a) contains a continuous solid line, connecting the incoming state k with the outgoing state k'. All diagrams contributing to the k-electron propagator have this property because H' conserves the number of k electrons. We refer to this as the base line of a diagram and draw

it as a straight horizontal line running from right to left.

It turns out that the most important subset of self-energy diagrams in the Kondo problem are those which contain no solid lines other than those appearing in the base line. We call these the parquet diagrams. It will be shown that our definition is slightly more general than that used by previous authors.[1,18]

By our choice of the z axis, the incoming k line has spin up. In parquet diagrams, we specify the spin direction of d lines by using the convention that $d\uparrow$ lines are drawn on the right-hand side of the direction of the base line and $d\downarrow$ lines on the left. Figure 1(a) can then be redrawn as in Fig. 1(b), where the given momenta and energy parameters are sufficient to determine the propagators completely.

Apart from convenience, this convention is useful because it enables us to identify uniquely the three kinds of vertices appearing in the diagrams with the three values that the matrix elements of the interaction H' (Eq. 2.2) can take, as illustrated by third-order parquet diagrams in Figs. 1(c) and 1(d). It is clear that a broken line crossing over a solid line represents a spin-flip interaction for which the amplitude is $(-2J)$, according to Eq. (2.2). The fork-shaped vertices, on the other hand, do not involve spin flip and the amplitude is $\pm J$, depending on whether the participating k and d lines have opposite or parallel spins. Figure 2 illustrates the identification for the cases occurring in parquet diagrams.

B. Diagrammatic expansion of the self-energy

We expand the self-energy as shown in Fig. 3 in a series of parquet diagrams. These can be subdivided in three groups: the first two contributions are the Hartree diagrams, the rest of the first four lines in Fig. 3 are the ordinary parquet

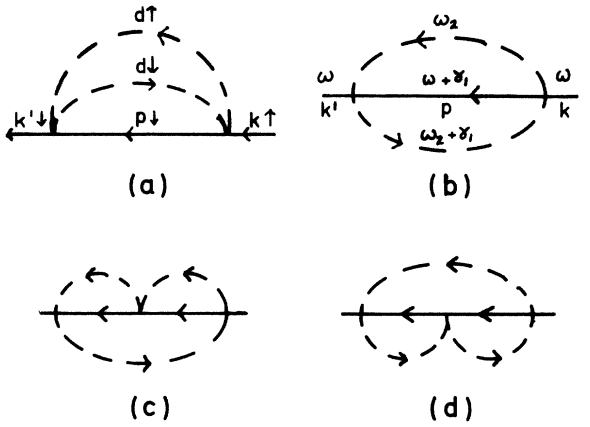

FIG. 1. Parquet graphs illustrating the conventions.

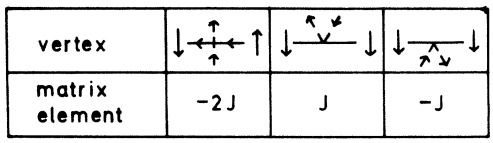

FIG. 2. Identification of vertices with matrix elements.

graphs, and the last line contain self-consistent parquet diagrams. Note that the term "parquet graphs", as used, for example, in Refs. 1, 16, and 18, includes only our "ordinary parquet graphs."

Various contributions to the self-energy have been neglected in Fig. 3. First, parquet diagrams with cross vertices (spin-flip interactions) in intermediate states, such as Fig. 4(a), are omitted. In Sec. III C a set of integral equations is derived which sums the set of ordinary parquet graphs of Fig. 3 exactly. The graphs with intermediate cross vertices can be included in these equations, but the formalism becomes considerably more complicated. When solving the integral equations, however, we restrict the sum at any rate to those graphs in which all intermediate conduction-electron states are on the same side of the Fermi surface. Under this assumption it is seen that all intermediate cross-vertex diagrams are anomalous and give no contribution. We therefore omit this type of graph from the start.

Second, no graphs containing self-consistently-

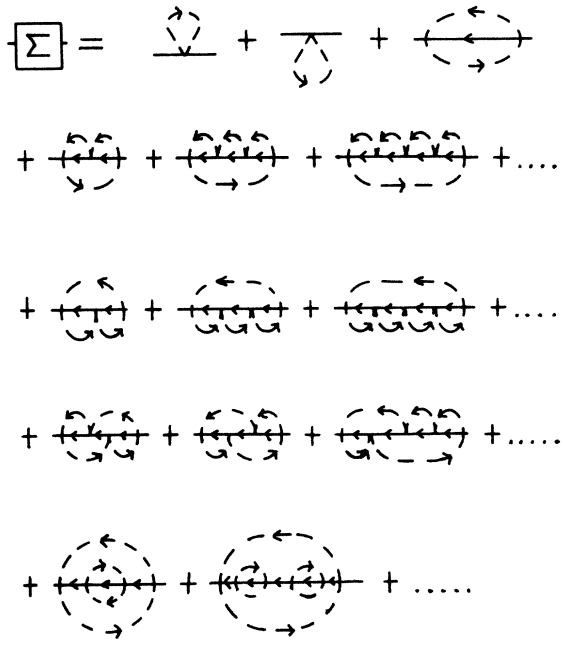

FIG. 3. Expansion of the self-energy.

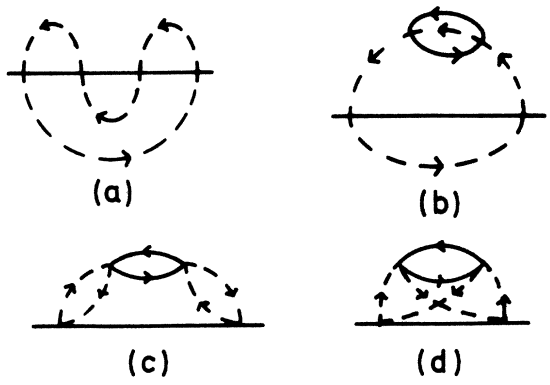

FIG. 4. Graphs which are omitted from the expansion.

clothed d lines [e.g., Fig. 4(b)] are included. Clothing of the d propagator gives rise to a shift in its energy ϵ_d. From the point of view of the pure Kondo model ϵ_d is an extra parameter at any rate, and as pointed out in Secs. II A and II B an arbitrary choice is made for its value in the specification of the limiting procedure. Therefore d-line clothing is not relevant in Kondo model calculations.

Third, nonparquet graphs, such as Figs. 4(c) and 4(d), in which the d-electron particle and hole are coupled by the conduction-electron background, are not taken into account. Earlier calculations, e.g., that of Abrikosov,[1] were restricted to the summation of ordinary parquet diagrams on the grounds that they contribute the highest order in the logarithmic divergence. As shown by the work of CM[16] and by the present work, the self-consistent parquet graphs which are of lower order in the logarithm, are equally important. The exclusion of nonparquet graphs can therefore be questioned and our excuse is one of simplicity.

C. Summation of ordinary parquet graphs

In the present paper, we approximate the self-energy Σ as the sum of the diagrams in the first four lines of Fig. 3 only. In the following paper the calculation is extended to include also the self-consistent parquet diagrams.

Let us define, for each ordinary parquet diagram X, its conjugate diagram $\tilde{X}$ as the diagram obtained by rotating X through 180° around its base line and reversing the directions of the arrows on all broken lines. Thus the second and third lines in Fig. 3 are, term for term, each other's conjugates.

A first partial summation can be performed by noting that $X=\tilde{X}$, as proved in Appendix A, so that pairs of conjugate diagrams can be added. Using this fact, we express (in Fig. 5) Σ in terms of a

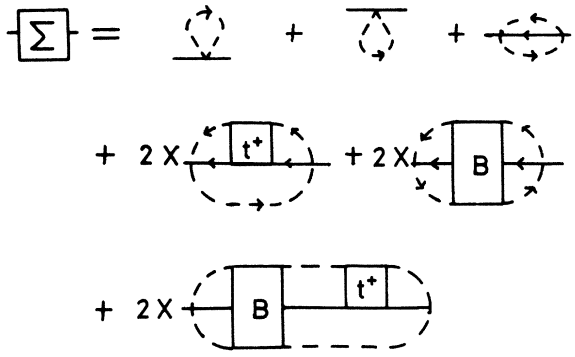

FIG. 5. Self-energy in terms of vertex parts t^* and B.

four-tailed vertex function t^+ and a six-tailed vertex function B, as defined by Fig. 6. It is seen that t^+ is a ladder approximation to the particle-particle vertex function, while B is composed of all asymmetric six-tailed vertex parts which begin with a fork-shaped vertex to the left of the base line and end with a fork-shaped vertex on the right of the base line.

Our expression for Σ appears more cumbersome than the corresponding one in the Abrikosov summation procedure.[1,18] However, the latter approach leads to an integral equation (for the vertex function) which is nonlinear and in addition involves multiple counting of self-energy graphs. An artificial restriction of certain energy parameters to the energy shell is then introduced in order to compensate for the multiple counting. Reference 18 (footnote 33) points out that the result is accurate at best to leading order in the logarithmic divergence, and even this is questioned for high-order contributions.

In contrast, we now proceed to derive integral equations for t^+ and B which are linear and which preserves the correct counting. The resulting expression for the self-energy is correct to all orders in the logarithm, within the parquet graph ap-

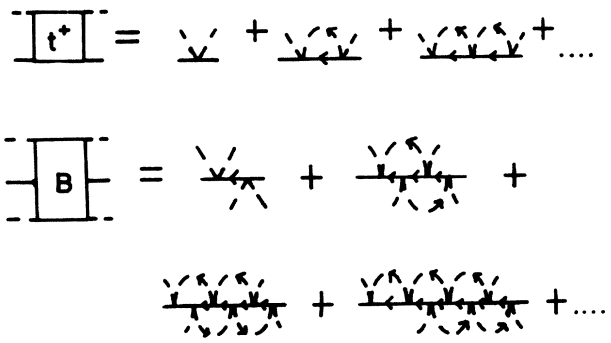

FIG. 6. Definitions of vertex parts t^+ and B.

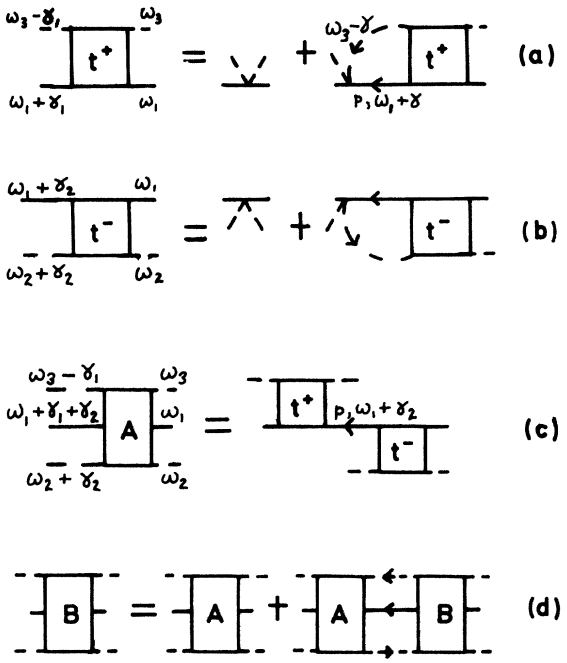

FIG. 7. Integral equations for the various vertex parts.

proximation.

By iteration it can be shown that t^+ satisfies the integral equation of Fig. 7(a). In Figs. 7(b) and 7(c) we define the auxiliary six-tailed vertex function A in terms of the particle-hole ladder vertex function t^-. Figure 7(d) states the central integral equation of our summation method, from which B is to be obtained. That B, as defined in Fig. 6, actually satisfies Fig. 7(d) is again proved by iteration. We stress that multiple counting in Fig. 7(d) is avoided because both A and B have asymmetrical structures.

It is possible to include also the type of graph of Fig. 4(a) in the sum by a slight reinterpretation of the same diagrammatic equations. The convention specifying the spin of the d lines must be dropped and the interaction represented in spin matrix formalism, as in the work of CM.[16] Figures 5–7 then represent an exact summation of the complete set of ordinary parquet graphs. For the sake of simplicity, however, we will not incorporate this generalization.

We use the conventions of Refs. 22 and 23 to translate Fig. 7 into algebraic equations in momentum space. Because J is a constant, it is easily shown that t^+ is a function of ω_1 and ω_3 only and Fig. 7(a) can be solved to give

$$-it^+(\omega_1,\omega_3)=-iJ[1+Js(\omega_1,\omega_3)]^{-1}\,, \tag{3.1}$$

where s is the "pair-bubble" function

$$s(\omega_1,\omega_3)=-\sum_p\int d\gamma\,(\gamma+\omega_1-\epsilon_p+i\delta_p)^{-1} \times(\gamma-\omega_3-U+i\delta_U)^{-1}(2\pi i)^{-1}\,, \tag{3.2}$$

where $\delta_p>0$ for $\epsilon_p>0$ and $\delta_U>0$ for $U>0$.

In order to calculate the function s by contour integration in Eq. (3.2), it is now necessary to specify the unperturbed ground state of the impurity spin. For $S=\uparrow$, $U>0$ (Sec. IIB) and $\delta_U>0$, so that the contour is closed at $-i\infty$ and we obtain

$$s_\uparrow(\omega_1+\omega_3+U)=\sum_{p<k_F}(\omega_1+\omega_3-\epsilon_p+U-i\delta)^{-1}. \tag{3.3}$$

At this stage we only make use of the sign of U and postpone taking its limiting value to Sec. IV A. Similarly for $S=\downarrow$ we find

$$s_\downarrow(\omega_1+\omega_3+U)=-\sum_{p>k_F}(\omega_1+\omega_3-\epsilon_p+U+i\delta)^{-1}\,. \tag{3.4}$$

We define two new functions $t_\uparrow$ and $t_\downarrow$ by the equation

$$t_{\uparrow;\downarrow}(\omega)=J[1+Js_{\uparrow;\downarrow}(\omega)]^{-1}\,. \tag{3.5}$$

Equation (3.1) then becomes

$$t^+_{\uparrow;\downarrow}(\omega_1,\omega_3)=t_{\uparrow;\downarrow}(\omega_1+\omega_3+U). \tag{3.6}$$

In a similar way the diagrammatic equation of Fig. 7(b) can be solved to give

$$t^-_{\uparrow;\downarrow}(\omega_1,\omega_2)=-t_{\uparrow;\downarrow}(\omega_1-\omega_2+U). \tag{3.7}$$

With the help of Eqs. (3.6) and (3.7), Fig. 7(c) can be directly translated to read

$$A_{\uparrow;\downarrow}(\omega_1,\omega_2,\omega_3,\gamma_2)=-t_{\uparrow;\downarrow}(\omega_1+\omega_3+\gamma_2+U)\,t_{\uparrow;\downarrow}(\omega_1-\omega_2+U)\sum_p(\omega_1+\gamma_2-\epsilon_p+i\delta_p)^{-1}, \tag{3.8}$$

while Fig. 7(d) represents the equation

$$B(\omega_1,\omega_2,\omega_3,\gamma_2)=A(\omega_1,\omega_2,\omega_3,\gamma_2) -\sum_{p,q}\int\frac{d\gamma_4\,d\gamma_5\,B(\omega_1,\omega_2,\omega_3,\gamma_4)t(\omega_1+\omega_3+\gamma_2+U)t(\omega_1-\omega_2+\gamma_5+U)}{(2\pi i)^2(\omega_2+\gamma_4-U+i\delta_U)(\omega_3-\gamma_5+U-i\delta_U)(\omega_1+\gamma_2+\gamma_5-\epsilon_q+i\delta_q)(\omega_1+\gamma_4+\gamma_5-\epsilon_p+i\delta_p)}\,. \tag{3.9}$$

The first step in the solution of Eq. (3.9) is to perform the γ_5 integral. We first consider the case where

$S=\downarrow$, then the integrand contains a factor $t_\downarrow(\gamma_5+\omega_1-\omega_2+U)$. According to Appendix B, this must be handled as a contour integration along a semicircle in the upper half-plane where $t_\downarrow$ is analytic, and we obtain

$$\int(\ )d\gamma_5=\sum_{p,q}\frac{t_\downarrow(\omega_1-\omega_2+\omega_3+2U)}{(\omega_1+\omega_3+\gamma_2-\epsilon_q+U+i\delta_q)(\omega_1+\omega_3+\gamma_4-\epsilon_p+U+i\delta_p)}$$
$$-\sum_{q<k_F,p}\frac{t_\downarrow(-\omega_2-\gamma_2+\epsilon_q+U)}{(\omega_1+\omega_3+\gamma_2-\epsilon_q+U+i\delta)(\gamma_4-\gamma_2+\epsilon_q-\epsilon_p+i\delta_p)}$$
$$+\sum_{p<k_F,q}\frac{t_\downarrow(-\omega_2+\gamma_4+\epsilon_p+U)}{(\omega_1+\omega_3+\gamma_4-\epsilon_p+U+i\delta)(\gamma_4-\gamma_2+\epsilon_q-\epsilon_p+i\delta_q)}\ . \tag{3.10}$$

When this expression is substituted back into Eq. (3.9), it is seen that because of the second and third sums in Eq. (3.10), the integrand of the γ_4 integral is no longer a separable function of γ_2 and γ_4. This is a major complication in the solution of the integral equation.

The troublesome terms in Eq. (3.10) can be traced back to the fact that the momenta p and q can be either above or below the Fermi momentum. In simple ladder diagrams (formed from the vertex functions t^+ and t^-) all intermediate conduction-electron propagators occur as part of a pair bubble and as seen from Eq. (3.4) this restricts them to particle states ($p>k_F$) for $S=\downarrow$. It is seen from Figs. 7(c) and 7(d) that the states p and q do not form part of pair bubbles and they are free to be either particle or hole states. We now make the approximation of restricting *all* intermediate conduction electron propagators to particle states for $S=\downarrow$ (or hole states for $S=\uparrow$) so that Eq. (3.10) is simplified to

$$\int(\ )d\gamma_5\simeq t_\downarrow(\omega_1-\omega_2-\omega_3+2U)$$
$$\times s_\downarrow(\omega_1+\omega_3+\gamma_2+U)s_\downarrow(\omega_1+\omega_3+\gamma_4+U). \tag{3.11}$$

The meaning of the approximation in terms of diagrams is best seen by considering the simplest non-ladder parquet diagram, Fig. 8. This Feynman graph is written as the sum of two Goldstone graphs in which particle and hole lines are explicitly distinguished. Similarly, each higher-order non-ladder parquet can be expanded as a (finite) series of Goldstone graphs, all of the same order in the interaction and in the logarithm. Our approximation selects only the first term, which has no kinks in the base line, from each series.

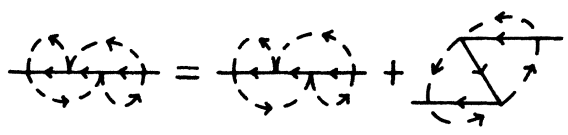

FIG. 8. Simplest non-ladder parquet as sum of Goldstone graphs.

The results of scaling theory[4] and of Nozieres *et al.*[25] on the x-ray problem indicates the importance of low-energy particle-hole excitations. Such states are included in the present theory in the $S=\uparrow$ graphs, where the base line consists entirely of hole lines, but multiple particle-hole states are excluded by the no kink approximation. Such intermediate states do occur in the self-consistent theory treated in the following paper.

Preliminary attempts to include the kinked graphs nevertheless do suggest that the analytic structure of our result is not drastically altered by them. This important point deserves further study, and work is presently in progress to include the rest of the Goldstone series in the summation. Meanwhile the approximation is justified by the fact that it enables us to solve the integral equation for B exactly, and that it leads to physically reasonable results. A similar approximation is made in the work of Suhl[3] and the close relationship (which will be explored in Sec. V) between our results and that of Abrikosov suggests that it is also implicit in the Abrikosov summation procedure.

It is also pointed out that while we now omit some graphs from the parquet series, the remainder is still summed exactly. Making use of Eq. (3.11) and suppressing superfluous arguments, Eq. (3.9) becomes

$$B_\downarrow(\gamma_2)=A_\downarrow(\gamma_2)+t_\downarrow(\omega_1+\omega_3+\gamma_2+U)$$
$$\times s_\downarrow(\omega_1+\omega_3+\gamma_2+U)t_\downarrow\int B_\downarrow, \tag{3.12}$$
$$\int B_\downarrow=\int d\gamma_4(2\pi i)^{-1}B_\downarrow(\gamma_4)$$
$$\times s_\downarrow(\omega_1+\omega_3+\gamma_4+U)(\omega_2+\gamma_4-U-i\delta)^{-1}\ . \tag{3.13}$$

Multiplying the integral equation (3.12) throughout by a factor

$$s_\downarrow(\omega_1+\omega_3+\gamma_2+U)(\omega_2+\gamma_2-U-i\delta)^{-1}$$

and integrating over γ_2 yields an algebraic equation for $\int B_\downarrow$. When this is solved and substituted back into Eq. (3.12), we find

$$B_{\downarrow}(\omega_1,\omega_2,\omega_3,\gamma_2)=t_{\downarrow}(\omega_1-\omega_2+U)t_{\downarrow}(\omega_1+\omega_3+\gamma_2+U)s_{\downarrow}(\omega_1+\gamma_2)$$
$$+t_{\downarrow}^2 s_{\uparrow}^2(1-t_{\downarrow}^2 s_{\uparrow}^2)^{-1}t_{\downarrow}(\omega_1-\omega_2+U)s_{\downarrow}(\omega_1-\omega_2+U)t_{\downarrow}(\omega_1+\omega_3+\gamma_2+U)s_{\downarrow}(\omega_1+\omega_3+\gamma_2+U). \quad (3.14)$$

In Eqs. (3.12) and (3.14) we have abbreviated $t_{\downarrow}(\omega_1-\omega_2+\omega_3+2U)$ to $t_{\downarrow}$, and similarly for $s_{\downarrow}$. The function $B_{\uparrow}$ can be calculated in a similar way. It is found that $-B(\omega_1,\omega_2,\omega_3,\gamma_2)$ is given by an expression similar to the right-hand side of Eq. (3.14), except that the $S=\downarrow$ subscripts are replaced by $S=\uparrow$.

D. Calculation of the self-energy

Having found the vertex functions, we can now compute the self-energy from Fig. 5. The latter is represented in algebraic form as

$$\Sigma=\Sigma_H+\Sigma_1+2\Sigma_2+2\Sigma_3+2\Sigma_4\,, \quad (3.15)$$

where Σ_H represents the Hartree graphs, Σ_1 the circle diagram of Fig. 1(b), Σ_2 the ladder graphs derived from t^+ and Σ_3 and Σ_4 the non-ladder parquets derived from B.

Each contribution is calculated by translating the corresponding graph into mathematical form [making use of Eqs. (3.5), (3.6), and (3.14)] and performing the integrations over intermediate energy parameters. We obtain

$$\Sigma_{H\uparrow;\downarrow}=\mp J, \quad (3.16)$$

$$\Sigma_{1\uparrow;\downarrow}=\pm 4J^2 s_{\uparrow;\downarrow}(\omega+2U), \quad (3.17)$$

where ω is the energy parameter of the entering propagator. Because of the conservation law at each vertex, the intermediate energy parameters ω_1, ω_2, ω_3 of Sec. III C is related to ω by the equation $\omega_1-\omega_2+\omega_3=\omega$. Consistently with the previous abbreviation we subsequently omit the argument $(\omega+2U)$ from t and s functions.

Straightforward contour integration gives the results

$$\Sigma_{2\uparrow;\downarrow}=\mp 4J^2 t_{\uparrow;\downarrow}s_{\uparrow;\downarrow}^2\,, \quad (3.18)$$

$$\Sigma_{3\uparrow;\downarrow}=\pm 4J^2 t_{\uparrow;\downarrow}^2 s_{\uparrow;\downarrow}^3(1-t_{\uparrow;\downarrow}s_{\uparrow;\downarrow})^{-1}\,, \quad (3.19)$$

$$\Sigma_{4\uparrow;\downarrow}=\mp 4J^2 t_{\uparrow;\downarrow}^3 s_{\uparrow;\downarrow}^4(1-t_{\uparrow;\downarrow}s_{\uparrow;\downarrow})^{-1}. \quad (3.20)$$

Substituting these values in Eq. (3.15) yields

$$\Sigma=\pm\left[J-4J^2 s(1-ts)(1+ts)^{-1}\right]\,,\quad +,\ -\ \text{for}\ S=\downarrow,\uparrow. \quad (3.21)$$

Using the value of t as given by Eq. (3.5), we find

$$\Sigma=\pm\left[J-4J^2 s(1+2Js)^{-1}\right],\quad +,\ -\ \text{for}\ S=\downarrow,\uparrow. \quad (3.22)$$

This expression is remarkably simple when the complex structure of the vertex function B, for example, is considered. We will now show that it also has a very simple graphical interpretation.

Consider first the following ladder approximation to the self-energy, using Eq. (3.5) for t:

$$\Sigma_L=\Sigma_H+\Sigma_1+\Sigma_2=\pm\left[J-4J^2 s(1+Js)^{-1}\right] \quad (3.23)$$

$$=\pm(J-4J^2 s+4J^3 s^2-4J^4 s^3+\cdots). \quad (3.24)$$

The diagrammatic expansion for Σ_L is just the first two lines of Fig. 3 and this can be identified term by term with the series of Eq. (3.24), on application of the following rules: (i) Associate with each k line a factor $(-s)$; (ii) associate with each vertex the magnitude of its interaction; and (iii) multiply the result with ± 1 for $S=\uparrow,\downarrow$.

Equation (3.22) for the full parquet self-energy is identical to Eq. (3.23) except for an extra factor 2 in the denominator. Its series expansion is the same as Eq. (3.24) except for an extra factor 2^n in the $(n+1)$th term, not counting the Hartree contribution. On the other hand, the $(n+1)$th ladder diagram has n forked vertices; when all parquet graphs are included, each fork can be either above or below the base line so that there are 2^n parquet graphs corresponding to the single ladder diagram. It follows that the three rules stated above for the ladder approximation also give a valid diagrammatic interpretation of Eq. (3.22).

IV. FINITE-TEMPERATURE SELF-ENERGY

A. Calculations in finite-temperature formalism

We now turn to the calculation of the self-energy at finite temperatures. As a first example let us consider Σ_1. Energy parameters are allocated in a similar way as in Fig. 1(b), using the symbol ω for a fermion energy parameter and γ for the transfer of energy parameter.

The conduction-electron propagator in Fig. 1(b) is given (in imaginary frequency formalism)[22] by $(i\omega_n+i\gamma_{m1}-\epsilon_p)^{-1}$, where we define

$$\omega_n=(2n+1)\pi\beta^{-1}\ \text{ and }\ \gamma_m=2m\pi\beta^{-1} \quad (4.1)$$

and a sum is taken over all positive- and negative-integer values of the indices n_i and m_i in intermediate states. All energies are measured from the Fermi surface, i.e., we take $\epsilon_F=0$. In the usual notation $\beta=1/K_B T$ where T is the temperature.

The finite-temperature version of Σ_1 is then found to be

$$\Sigma_1=-4J^2\sum_p\left[f(\epsilon_p)-f(U)\right]\left[f(U)+g(\epsilon_p-U)\right]$$
$$\times(i\omega_n-\epsilon_p+2U)^{-1}; \quad (4.2)$$

$$f(z)=(e^{\beta z}+1)^{-1},\quad g(z)=(e^{\beta z}-1)^{-1} \quad (4.3)$$

and we have used identities like $g(i\omega_n+z)\equiv -f(z)$, etc.

The self-energy for a specific impurity-spin projection is found from Eq. (4.2) by application of the limiting procedure in Sec. IIB. Because we are working in momentum space, U occurs in the denominator of Eq. (4.2) and taking the infinite limit causes problems. However, the intention of the infinite limit is simply to ensure a "pure" occupation of the d states, and the same result can be obtained for finite U by using the zero-temperature limit of the d-state distribution functions. Once this is done U must be eliminated from the answer because it is an artifical parameter which was introduced in the second quantization of S and does not appear in the pure Kondo model. It is an unimportant additive constant in the numerator and we simply make it zero. Our limiting procedure can then be summarized in the following prescription:

For $S=\uparrow,\downarrow$ let $U\to\pm 0$; but wherever the temperature-dependent statistical factor $e^{\beta U}$ appears, the limit $\beta\to\infty$ is taken in such a way that

$$|\beta U|\to\infty. \tag{4.4}$$

Application of this prescription to Eq. (4.2) yields

$$\Sigma_{1\uparrow}=4J^2\sum_p f(\epsilon_p)(i\omega_n-\epsilon_p)^{-1}\equiv 4J^2 s_\uparrow(i\omega_n), \tag{4.5}$$

$$\Sigma_{1\downarrow}=-4J^2\sum_p [f(\epsilon_p)-1](i\omega_n-\epsilon_p)^{-1}\equiv -4J^2 s_\downarrow(i\omega_n)\ . \tag{4.6}$$

The functions $s_\uparrow$ and $s_\downarrow$ are defined by the identities in Eqs. (4.5) and (4.6). We use the same symbols as for the pair-bubble functions at zero temperature, as it is easily seen by comparison with Eqs. (3.3) and (3.4) that the two sets are connected by the standard analytic continuation $i\omega_n\to\omega\pm i\delta$ and taking the zero-temperature limit of the Fermi function $f(\epsilon_p)$. Equations (4.5) and (4.6) for $\Sigma_{1\uparrow,\downarrow}$ correspond exactly to their zero-temperature counterpart, Eq. (3.17).

Note that while in Eq. (4.2) the impurity spin gives a contribution to the temperature dependence of the self-energy, this is eliminated by the limiting procedure (4.4). In Eqs. (4.5) and (4.6) the full temperature dependence is carried by the Fermi sea of conduction electrons. As pointed out in Sec. IIB, this is as required by the pure Kondo model.

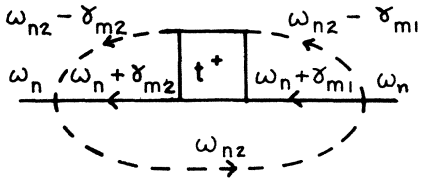

FIG. 9. Allocation of energy parameters in ladder contribution Σ_2 to self-energy.

B. Ladder approximation at $T>0$

We treat the ladder approximation at finite temperatures along similar lines as at $T=0$. Our calculation of the t functions in Sec. IIIC is considerably simplified by the fact that all intermediate vertices in parquet graphs are taken to be non-spin-flip. This, in turn, is valid within our pure-particle or pure-hole intermediate state approximation because diagrams containing anomalous d lines vanish and can be omitted *a priori*.

At finite temperatures, anomalous diagrams must, in general, be taken into account. However, application of the prescription (4.4) yields the zero-temperature limit of the d propagators. According to the Kohn-Luttinger-Ward theorem (see Ref. 22, p. 289), diagrams with anomalous d lines can then be neglected, provided that the Lagrange multipliers $\mu_{d\uparrow}$ and $\mu_{d\downarrow}$ are adjusted to give the correct occupation numbers in the *unperturbed* system. This is exactly the implication of Eqs. (2.9), (2.10), and (4.4).

The integral equations of Figs. 7(a) and 7(b) can now be solved in an exactly analogous way to the zero temperature case, and we obtain

$$t^+_{\uparrow;\downarrow}(\omega_{n1},\omega_{n3})=t_{\uparrow;\downarrow}(i\omega_{n1}+i\omega_{n3}+U), \tag{4.7}$$

$$t^-_{\uparrow;\downarrow}(\omega_{n1},\omega_{n2})=-t_{\uparrow;\downarrow}(i\omega_{n1}-i\omega_{n2}+U), \tag{4.8}$$

$$t_{\uparrow;\downarrow}(i\omega_n)=J\,[1+Js_{\uparrow;\downarrow}(i\omega_n)]^{-1}\ . \tag{4.9}$$

These equations are again related to their zero-temperature counterparts, Eqs. (3.5)–(3.7), by an analytic continuation of their zero-temperature limits. Using Eq. (4.7), the ladder contribution Σ_2 to the self-energy is calculated with energy parameters allocated as in Fig. 9. After performing the sums over the m's by the standard Poisson procedure (see below) we find

$$\Sigma_2=\frac{4J^2}{\beta}\sum_{p,q,n2}\frac{[f(\epsilon_p)-f(U)][f(\epsilon_q)-f(U)]t(i\omega_n+i\omega_{n2}+U)}{(i\omega_{n2}-U)(i\omega_n+i\omega_{n2}-\epsilon_p+U)(i\omega_n+i\omega_{n2}-\epsilon_q+U)}\ . \tag{4.10}$$

To carry out the sum over $n2$, we represent t in terms of a spectral function Q:

$$t(i\omega_n+U)=\int_{-\infty}^{\infty}d\omega\,Q(\omega)(i\omega_n+U-\omega)^{-1}\ , \tag{4.11}$$

$$Q(\omega)=-\pi^{-1}\,\mathrm{Im}\,t(\omega+i\delta)\ . \tag{4.12}$$

Using Eq. (4.11), the Poisson summation formula,[22] which states that for a suitable function F

$$\beta^{-1}\sum_n F(i\omega_n) = \text{sum of residues of } F(z)f(z) \text{ at the poles of } F(z) \qquad (4.13)$$

can be applied to Eq. (4.10). The four terms arising from the four poles of the summand of Eq. (4.10) can be divided into two groups: the single term derived from the $i\omega_{n2} = U$ pole and which contains an over-all factor $f(U)$, and the other three terms, all containing over-all factors of the form $f(\cdots - U)$.

To find $\Sigma_{2\downarrow}$, we take the limit $\beta U \to -\infty$ and the last-mentioned group of terms vanishes, giving

$$\Sigma_{2\downarrow} = 4J^2 t_\downarrow s_\uparrow^2 , \qquad (4.14)$$

where $t_\downarrow$ stands for $t_\downarrow(i\omega_n)$, etc.

In the opposite limit $\beta U \to +\infty$, it is the single term which vanishes and some tedious algebra is involved in adding the three remaining terms. The result is simple, however:

$$\Sigma_{2\uparrow} = -4J^2 t_\uparrow s_\uparrow^2 . \qquad (4.15)$$

Comparison of the last two equations with Eq. (3.18) shows that again there is exact correspondence with the zero-temperature formalism.

The calculation of Σ_2 illustrates a general feature of finite-temperature computations. In the zero-temperature formalism, similar but separate calculations yield the results for $S = \uparrow$ and $S = \downarrow$. The finite temperature formalism treats both cases simultaneously, but as above it turns out that $S = \downarrow$ quantities are the simplest to calculate. In Sec. IV C we will therefore concentrate on the $S = \downarrow$ case. This can be done by simply ignoring poles of the form $i\omega_n = \cdots - U$ in Poisson summations, as their residues vanish in any case in the infinite limit. The $S = \uparrow$ results are obtained by comparison with the zero-temperature results.

C. Non-ladder parquet contributions to the self-energy

The $T > 0$ formalism is next used to translate Figs. 7(c) and 7(d) into equations similar to Eqs. (3.8) and (3.9), respectively. We encounter a sum over γ_{m5} which can be performed to give (in the $S = \downarrow$ case)

$$\sum_{m5} = \sum_{p,q} \left(\frac{f(U)t(i\omega_{n1} - i\omega_{n2} + i\omega_{n3} + 2U)}{(i\omega_{n1} + i\omega_{n3} + i\gamma_{m2} - \epsilon_q + U)(i\omega_{n1} + i\omega_{n3} + i\gamma_{m4} - \epsilon_p + U)} - \frac{f(\epsilon_q)t(-i\omega_{n2} - i\gamma_{m2} + \epsilon_q + U)}{(i\omega_{n1} + i\omega_{n3} + i\gamma_{m2} - \epsilon_q + U)(i\gamma_{m4} - i\gamma_{m2} + \epsilon_q - \epsilon_p)} \right.$$
$$\left. + \frac{f(\epsilon_p)t(-\omega_{n2} - i\gamma_{m4} + \epsilon_p + U)}{(i\omega_{n1} + i\omega_{n3} + i\gamma_{m4} - \epsilon_p + U)(i\gamma_{m4} - i\gamma_{m2} + \epsilon_q - \epsilon_p)} \right) . \qquad (4.16)$$

Once more, this agrees with the zero-temperature result, Eq. (3.10). The agreement enables us to write the appropriate approximation (for the exact solution of the sum equation for B), namely

$$\sum_{m5} \approx \sum_{p,q} \frac{[f(U) - f(\epsilon_p)][f(U) - f(\epsilon_q)]t(i\omega_{n1} - i\omega_{n2} + i\omega_{n3} + 2U)}{(i\omega_{n1} + i\omega_{n3} + i\gamma_{m2} - \epsilon_q + U)(i\omega_{n1} + i\omega_{n3} + i\gamma_{m4} - \epsilon_p + U)} \qquad (4.17)$$

This approximation which has an artificial appearance in the present formalism, is justified in the same way as at $T = 0$ (section 3.3), and as shown there it has a simple diagrammatic interpretation as a "no kink" approximation.

The rest of the calculation of B and of the self-energy contributions derived from it is performed along similar lines as at $T = 0$ and Eqs. (3.19)–(3.22) are all found valid with the t and s functions now interpreted as finite temperature functions.

V. RESISTIVITY IN VARIOUS APPROXIMATIONS

Having calculated the parquet graph self-energy, we are now in a position to find the single-particle T matrix from Eq. (2.15) and the resistivity from Eq. (2.18). Before doing so, we will explore the relationship of our work with various other non-self-consistent calculations of the resistivity by considering a number of simplified approximations.

The first simplification is to approximate the T matrix by the first term in its expansion, namely the (irreducible) self-energy. This is done by all the previous authors referred to in this section. Second, the self-energy can be represented by various more-restricted graphical sums.

A. Finite-order perturbation theory

When only terms up to third order in the interaction is included, we find

$$\Sigma_{\uparrow;\downarrow} = \mp (J - 4J^2 s_{\uparrow;\downarrow} + 4J^3 s_{\uparrow;\downarrow}^2) , \qquad (5.1)$$

where, as before, $s \equiv s(i\omega_n)$, so that Eq. (5.1) gives the self-energy in the imaginary frequency domain and we must make the analytic continuation $i\omega_n \to \omega + i\delta$ to obtain the physical T matrix and self-energy. According to Eq. (2.18) we only need the T matrix at the Fermi surface, $\omega = 0$, and the s functions in this point is given according to Appendix B by

$$s_{\uparrow,\downarrow}(0 + i\delta) \simeq \rho \ln \beta D \mp \tfrac{1}{2} i\pi\rho , \qquad (5.2)$$

where ρ and D are defined in Sec. II A. Combining

Eqs. (2.18), (5.1), and (5.2), we obtain

$$R/R_u = 2J^2\pi^2\rho^2(1 - 4J\rho \ln\beta D) \ . \quad (5.3)$$

We first compare this with the expression found by Kondo[26] with ordinary perturbation theory in the pure Kondo model. Taking into account that $J(\text{Kondo}) = 2NJ$ (see Sec. II A) and $\rho(\text{Kondo}) = \rho/N$ in our notation, Eq. (4.13) of Ref. 26 becomes

$$R/R_u = 2J^2\pi^2\rho^2(1 - 8J\rho \ln\beta D) \ \text{(Kondo)}. \quad (5.4)$$

This is identical to our expression, Eq. (5.3), except for an extra factor 2 in the brackets. From Eqs. (14.7) and (14.8) of Ref. 26, it becomes clear that this discrepancy results from the inclusion of irrelevant non-forward-scattering terms in the work of Kondo.

A third-order expression is also derived by Cheung and Mattuck[16] (CM). From their Eq. (1) it follows that $J(\text{CM}) = 4NJ$ in our notation, and Eq. (50) of Ref. 16 becomes

$$R/R_u = \tfrac{3}{4}J^2\pi^2\rho^2(1 - 4J\rho \ln\beta D) \ \text{(CM)} \ . \quad (5.5)$$

This expression differs from Eq. (5.3) by a factor $\frac{3}{8}$. The origin of this difference (which we will also find in the work of Abrikosov) is not clear, but comparison of Eqs. (5.3)–(5.5) appears to support the idea that our method corresponds more closely to the pure Kondo model than the previous approaches.

The qualitative behavior of the resistivity R given by Eq. (5.3) is illustrated for $J < 0$ by curve (a) in Fig. 10. As shown by Kondo[19] the high-temperature tail gives a reasonable account of the depth and position of the resistivity minimum observed in dilute magnetic alloys. At low temperatures, however, R exceeds the theoretical maximum value R_u and diverges at $T \to 0$.

B. Ladder approximation

The self-energy is next approximated by a sum of all ladder graphs, given in the notation of Sec. III D by

$$\Sigma = \Sigma_H + \Sigma_1 + 2\Sigma_2 \ . \quad (5.6)$$

This represents the graphs in the first three lines of Fig. 3. Making use of Eqs. (3.16)–(3.18) and (5.2) we find

$$R/R_u = 2J^2\pi^2\rho^2\{2\,[(1 + J\rho \ln\beta D)^2 + \tfrac{1}{4}J^2\pi^2\rho^2]^{-1} - 1\} \ . \quad (5.7)$$

Equation (5.7) is represented by curve (b) in Fig. 10. In the high-temperature region it approaches the perturbation theory result; but instead of diverging, a smooth maximum and a decreasing behavior near $T = 0$ is exhibited. Some unphysical traits remain, however: the maximum resistivity is $14R_u$ instead of R_u, and at low temperatures negative values are attained.

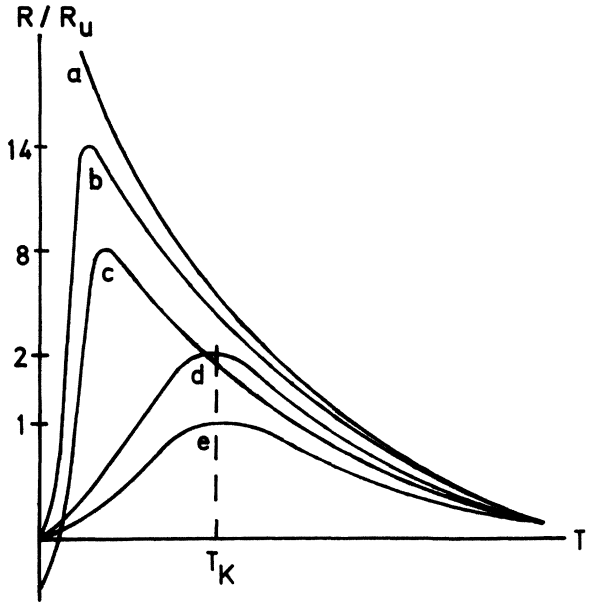

FIG. 10. Qualitative behavior of various approximations for the Kondo resistivity as function of temperature for $J < 0$. (a) Third-order perturbation theory; (b) full ladder approximation; (c) simple ladder approximation; (d) self-energy parquet approximation; (e) T-matrix parquet approximation.

The approximation can actually be improved by a simplified ladder approximation which includes only the particle-particle (or only particle-hole) graphs, but not both. Equation (3.23) is used for the self-energy, and we obtain

$$R/R_u = 2J^2\pi^2\rho^2[(1 + J\rho \ln\beta D)^2 + \tfrac{1}{4}J^2\pi^2\rho^2]^{-1} \ . \quad (5.8)$$

The maximum value is now decreased to $8R_u$ [see Fig. 10(c)] and no negative resistivity occurs. Furthermore, Eq. (5.8) resembles the full parquet approximation result, which we derive in the next section [Eq. (5.11)] so closely, that we suggest that this simple ladder approximation can be used as a first approximation in subsequent calculations.

A full ladder approximation corresponding to Eq. (5.6) was also used by CM. In our notation, Eq. (47) of Ref. 16 reads

$$\frac{R}{R_u} = \tfrac{3}{4}J^2\pi^2\rho^2\left(\frac{2(1 + 3J^2\rho^2 \ln^2\beta D)}{(1 + 3J\rho \ln\beta D)^2(1 - J\rho \ln\beta D)^2} - 1\right) \ \text{(CM)}. \quad (5.9)$$

Equation (5.9) has obvious similarities to our expression, Eq. (5.7), and has a similar numerical behavior at high temperatures, but there are two important differences. In the first instance, for $J < 0$, Eq. (5.9) diverges at a certain critical temperature, whereas Eq. (5.7) attains a finite maximum. Second, Eq. (5.7) decreases monotonically

at $T \to 0$ for $J > 0$, but Eq. (5.9) diverges at a second critical temperature. This extra divergence is also found in Ref. 17, but not in pure Kondo model calculations. In fact it can be traced back to the inclusion of diagrams which would be "anomalous" in the pure Kondo model, by the TO limiting procedure (Sec. II A). It is a sympton of the fact that the two approaches are not completely equivalent.

C. Parquet approximation

We have already found the sum of parquet self-energy graphs, Eq. (3.22). From this it follows that

$$\Sigma_\uparrow + \Sigma_\downarrow = 4J^2[s_\uparrow(1+2Js_\uparrow)^{-1} - s_\downarrow(1+2Js_\downarrow)^{-1}] . \tag{5.10}$$

Combination of this result with Eqs. (2.18) and (5.2) yields

$$R/R_u = 2J^2\pi^2\rho^2[(1+2J\rho\ln\beta D)^2 + J^2\pi^2\rho^2]^{-1} . \tag{5.11}$$

Once again, for $J < 0$, we find a curve [Fig. 10(d)] which in the high-temperature region rises logarithmically as the temperature decreases, reaches a maximum and decreases to zero at $T = 0$. The temperature at which the maximum is attained is defined as the Kondo temperature

$$T_K = (D/K_B)\, e^{1/2J\rho} \tag{5.12}$$

and the maximum value is $R = 2R_u$. With the help of Eq. (5.12) we can eliminate the three unknown quantities J, ρ, and D in Eq. (5.11) in favor of a single unknown T_K, and find

$$R/R_u = 2\pi^2[4\ln^2(T/T_K) + \pi^2]^{-1} . \tag{5.13}$$

Equation (5.11) is in a suitable form for comparison with Abrikosov's result[1]

$$R/R_u = \tfrac{3}{4}J^2\pi^2\rho^2(1+2J\rho\ln\beta D)^{-2} \quad \text{(Abrikosov)}. \tag{5.14}$$

To obtain this expression from Eq. (24) of Ref. 1, we have made use of the fact that Abrikosov's $J_1 = 2NJ$ and that our ρ is the density of states at the Fermi level, $\rho = 3Nz/2\epsilon_F$.

Far from the Kondo temperature $(1+2J\rho\ln\beta D)$ is a large parameter and Eq. (5.11) can be expanded as the series

$$R/R_u = 2J^2\pi^2\rho^2(1+2J\rho\ln\beta D)^{-2} - 2J^4\pi^4\rho^4(1+2J\rho\ln\beta D)^{-4} + \cdots . \tag{5.15}$$

The first term in the expansion is the Abrikosov expression, except for the factor $\frac{3}{8}$ mentioned before. It becomes clear, therefore, that the Abrikosov formula is an approximation (valid far from the Kondo temperature) to the parquet sum expression [Eq. (5.11)]. In fact, if Eq. (5.15) is expanded as a power series in J, it is easily seen that the Abrikosov term contributes the highest order in the logarithm for a given order in J. This is an explicit confirmation of Abrikosov's claim that his procedure sums the parquet series correctly to leading order in the logarithm—provided that our no-kink approximation [Eq. (3.11)] is also implicit in Abrikosov's work.

At the Kondo temperature, the Abrikosov resistivity diverges for $J < 0$ while Eq. (5.11) only attains a smooth maximum. This is a clear indication of the importance of the terms of lesser order in the logarithm which are included exactly in Eq. (5.11).

Finally a comparison is made with the non-self-consistent high-temperature form derived by Nagaoka[2] [see also Eq. (49) of Ref. 16]:

$$R/R_u = \tfrac{3}{4}J^2\pi^2\rho^2(1+4J\rho\ln\beta D)^{-1} \quad \text{(Nagaoka)} . \tag{5.16}$$

This also diverges at a critical temperature. In fact, Eq. (5.16) is only an approximation of the Abrikosov form, obtained by neglecting the quadratic term in the numerator of Eq. (5.14). It reproduces the first two terms in a series expansion in J correctly, but higher-order terms deviates from the expansion of Eq. (5.11). A similar linearization of the numerator also occurs in the self-consistent Nagaoka theory, as is shown in a subsequent paper.

D. T-matrix parquet approximation

Despite its success in improving on previous results and the elimination of divergences, the parquet-sum self-energy approximation is still unsatisfactory because a resistivity higher than R_u still occurs, and because at $T = 0$ the resistivity approaches zero instead of saturating to R_u, as observed experimentally. Within the framework of the present calculation we can still make one more refinement: the full T matrix is calculated from Eq. (2.15) and substituted in Eq. (2.18) for calculating the resistivity.

This approach only partially succeeds in solving the above-mentioned problems. A complicated expression is obtained for R, having the qualitative behavior of Fig. 10(e). The resistivity at T_K is given by

$$R/R_u = (2+J^2\pi^2\rho^2)/(3+J^2\pi^2\rho^2) \tag{5.17}$$

and is also approximately the maximum value, and the zero-temperature value is

$$R/R_u = J^2\pi^2\rho^2(1+J^2\pi^2\rho^2)^{-1} . \tag{5.18}$$

It is seen that R does not exceed R_u any more, and for $|J| \to \infty$ saturation at $R = R_u$ is obtained. However, a realistic order of magnitude for T_K is 10 K, so that according to Eq. (5.12) we expect $(J\rho) \simeq -0.05$ and the $T = 0$ limit of R/R_u is virtually zero.

In a subsequent paper it is shown that this problem is only resolved by a fully self-consistent calculation. For this reason we do not even attempt a numerical fit of the non-self-consistent theory to experimental data.

VI. CONCLUSION

The main result of our study is Eq. (5.13), for R, the Kondo contribution to the resistivity, as a function of the temperature T. This is derived by approximating the T matrix by the self-energy and the self-energy by a selected sum of ordinary parquet graphs. We have shown that finite-order perturbation theory, various ladder approximations, including that of CM,[16] Nagaoka's high-temperature formula,[2] and the work of Abrikosov,[1] are successive approximations to our parquet-sum expression.

Unlike these approximations, Eq. (5.13) shows no divergence at the Kondo temperature. This leads to the conclusion that the divergence previously found when working to logarithmic accuracy, is cancelled when the less divergent terms are included in the summation and is not inherent in the ordinary (non-self-consistent) parquet sum.

In this respect we differ from the conclusion of Nozières *et al.*[25] in connection with the x-ray problem and of Cheung and Mattuck[16] for the Kondo problem, that a self-consistent calculation is necessary to remove the divergence. The importance of self-consistency is clearly illustrated by scaling theory.[4] It is found that the effective interaction with electrons near the Fermi level is strongly renormalized by interaction of the localized moment with electrons at higher energies. Consequently, at low temperatures, where the low-lying states play an important role, the conduction-electron self-energy cannot be calculated from the unrenormalized interaction as in the present paper.

Both these theoretical considerations and the fact that the ordinary parquet sum is found insufficient to give the observed saturation of the resistivity at zero temperature, indicate the need for the self-consistent calculation which is performed in the subsequent paper.

ACKNOWLEDGMENT

The author is deeply indebted to Professor R. H. Lemmer for numerous valuable discussions of the work, and for his interest and encouragment while it was in progress.

APPENDIX A: PROOF THAT $X=\tilde{X}$

We prove here that the conjugate diagram $\tilde{X}$ obtained by rotating a parquet diagram X through 180° around its base line, is equal to X in the finite-temperature formalism. A similar proof holds for $T=0$.

Starting off with X in which valid energy parameters (i.e., satisfying conservation relations at each vertex) have been allocated to each line, it is seen that a valid allocation in the conjugate diagram is obtained by changing the sign of the energy parameter whenever the direction of the arrow on a line is changed by the transformation $X \to \tilde{X}$. Therefore, for each factor $\mathcal{G}_0(d\downarrow, \omega_n)$ in X, a factor $\mathcal{G}_0(d\downarrow, -\omega_n)$ appears in $\tilde{X}$. Now, making use of Eq. (2.10), it is seen that

$$\mathcal{G}_0(d\downarrow, \omega_n) = (i\omega_n - U)^{-1} = -\mathcal{G}_0(d\downarrow, -\omega_n) \ . \qquad \text{(A1)}$$

It follows that $\tilde{X}$ contains a factor (-1) relative to X, for each of its d lines. In the transformation all the fork-shaped vertices are inverted, so that each contributes an additional factor (-1) according to Fig. 2. If X has m forked vertices, it has $(m+2)$ d lines, so that

$$\tilde{X} = (-1)^{m+(m+2)} X = X. \qquad \text{(A2)}$$

APPENDIX B: CALCULATION OF s FUNCTIONS

$T=0$. Consider the function $s_\downarrow(\omega)$, defined as in Eq. (3.4). We approximate the sum by an integral over energies, weighted by a block-function density of states, as described below Eq. (2.2). This yields

$$s_\downarrow(\omega) = -\rho \ln[(\omega - \epsilon_F + i\delta)(\omega - D + i\delta)^{-1}] \ . \qquad \text{(B1)}$$

Integration of $s_\downarrow(\omega)$ with respect to ω can be performed by introducing the analytic continuation $\omega + i\delta \to z$, where z is a complex variable. $s_\downarrow(z)$ is analytic except for a branch line along part of the real axis. Integration of $s_\downarrow(\omega)$ over all real values of ω is therefore equivalent to a contour integration of $s_\downarrow(z)$ along a line just off the real axis in the upper half-plane and closed by a semicircle at $+i\infty$.

It is clear from Eq. (3.5) that $t_\downarrow(z)$ has the same branch line as $s_\downarrow(z)$, and in addition a first-order pole. Eq. (B1) can be used to show that this pole is also on the real axis so that the same contour $C_\downarrow$ as described above is used to integrate $t_\downarrow(\omega)$. This fact is used to obtain Eq. (3.10).

In a similar way it follows that integration over the arguments of $s_\uparrow$ and $t_\uparrow$ functions is performed along a contour $C_\uparrow$ given by the mirror image (in the real axis) of $C_\downarrow$. It can be shown that the analytic properties derived here is independent of the form chosen for the density of states, as long as $\int J\rho(\epsilon)\,d\epsilon$ is finite. This is true for any realistic interaction and density of states.

$T>0$. For calculating the self-energy of a k-electron particle in real energy space, the function $s_\uparrow(i\omega_n)$ of Eq. (4.5) must be analytically continued to

$$s_1(\omega + i\delta) = \sum_p f(\epsilon_p)(\omega - \epsilon_p + i\delta)^{-1} . \quad \text{(B2)}$$

We change the sum into an integral and use the block density of states to obtain

$$s_1(\omega + i\delta) = \rho P \int_{-D}^{D} f(\epsilon)(\omega - \epsilon)^{-1} d\epsilon - i\pi\rho f(\omega) . \quad \text{(B3)}$$

We approximate the function $f(\epsilon)$ [defined by Eq. (4.3)] which occurs in the principal-value integral by the inclined step function

$$f(\epsilon) \simeq \begin{cases} 1, & \text{for } \beta\epsilon < -2 \\ \frac{1}{2} - \frac{1}{4}\beta\epsilon, & -2 \leq \beta\epsilon \leq 2 \\ 0, & \beta\epsilon > 2 . \end{cases} \quad \text{(B4)}$$

This deviates significantly from the exact value only in a region of order $\Delta\epsilon = 1/\beta$ centered around $\epsilon = 2/\beta$. Substituting Eq. (B4) in Eq. (B3), we find

$$P\int \simeq 1 + \ln\beta(\omega + D) + \tfrac{1}{4}(\beta\omega - 2)\ln|\beta\omega - 2| - \tfrac{1}{4}(\beta\omega - 2)\ln(\beta\omega + 2) \quad \text{(B5)}$$

$$\simeq \ln\beta(\omega + D). \quad \text{(B6)}$$

Numerical calculations of Eq. (B3) for room temperature ($\beta = 40$) shows that Eq. (B5) overestimates the integral by 3% at $\omega = 0$ and improves with increasing values of $|\omega|$. Equation (B6) which is valid for $\omega \simeq 0$ underestimates the integral by 2%. Both approximations improve with decreasing temperature. Our final result for the s_1 function at the Fermi level ($\omega = 0$) is found from Eqs. (B3) and (B6):

$$s_1(0 + i\delta) \simeq \rho \ln\beta D - \tfrac{1}{2} i\pi\rho . \quad \text{(B7)}$$

The function $s_1(0 + i\delta)$ can be calculated in a similar way.

---

*This work is based on a part of a Ph.D. thesis submitted by the author to the Physics Dept., Rand Afrikaans University, Johannesburg (December 1972).

†Research supported by a bursary from the South African Council for Scientific and Industrial Research, Pretoria.

[1]A. A. Abrikosov, Physics 2, 5 (1965).
[2]Y. Nagaoka, Phys. Rev. 138, A1112 (1965).
[3]H. Suhl, Phys. Rev. 138, A515 (1965).
[4]P. W. Anderson, Comm. Solid State Phys. 3, 73 (1973).
[5]D. R. Hamann, Phys. Rev. 158, 570 (1967).
[6]J. Zittarz, Z. Phys. 217, 155 (1968).
[7]J. Zittarz and A. Müller-Hartmann, Z. Phys. 212, 380 (1968).
[8]D. C. Mattis, Phys. Rev. Lett. 19, 1478 (1967).
[9]H. Keiter, Z. Phys. 213, 466 (1968).
[10]G. E. Stedman, Phys. Lett. A 35, 425 (1971).
[11]H. Keiter, Phys. Lett. A 36, 257 (1971).
[12]T. D. Schultz and P. C. Kwok, Phys. Lett. A 39, 402 (1972).
[13]H. C. Fogedby, Phys. Lett. A 41, 103 (1972).
[14]K. K. Murata, Phys. Lett. A 42, 151 (1972).
[15]W. S. Verwoerd, Phys. Lett. A 43, 535 (1973).
[16]C. Y. Cheung and R. D. Mattuck, Phys. Rev. B 2, 2735 (1970).
[17]F. Takano and T. Ogawa, Prog. Theor. Phys. 35, 343 (1966).
[18]S. D. Silverstein and C. B. Duke, Phys. Rev. 161, 456 (1967).
[19]J. Kondo, Progr. Theor. Phys. 32, 37 (1964).
[20]U. Larsen, Z. Phys. 256, 65 (1972).
[21]A simple derivation of Eq. (2.2) from first principles is given by U. Larsen, J. Phys. C 4, 1835 (1971).
[22]Our notation corresponds as closely as possible to that of A. L. Fetter and J. D. Walecka, *Quantum Theory of Many-Particle Systems* (McGraw-Hill, New York, 1971).
[23]R. D. Mattuck, *A Guide to Feynman Diagrams in the Many-Body Problem* (McGraw-Hill, New York, 1967).
[24]J. M. Ziman, *Principles of the Theory of Solids* (Cambridge U. P., London, 1965).
[25]B. Roulet, J. Gavoret, and P. Nozières, Phys. Rev. 178, 1072 (1969); and P. Nozières, J. Gavoret, and B. Roulet, Phys. Rev. 178, 1084 (1969).
[26]J. Kondo, Solid State Phys. 23, 183 (1969).